Study of ^{6}Li+^{7}Li anomalous large-angle scattering*

Zhi-Hao Sun,[1] Hao-Yang Fan,[1] Yi-Ting E,[1] Hai-Rui Guo,[1,†] Tao Ye,[1] Wei-Li Sun,[1] Xu Han,[1] Wen-Di Chen,[1] Yang-Jun Ying,[1] Yong-Li Xu,[2] Dong-Hong Zhang,[2] and Yin-Lu Han[3]

[1] *Institute of Applied Physics and Computational Mathematics, Beijing 100094, China*
[2] *College of Physics and Electronic Science, Shanxi Datong University, Datong 037009, China*
[3] *Key Laboratory of Nuclear Data, China Institute of Atomic Energy, Beijing 102413, China*

This study investigates the mechanism of ^{6}Li+^{7}Li anomalous large-angle scattering. First, elastic scattering is analyzed using an optical model with the São Paulo potential, and inelastic scattering to the first excited state of ^{7}Li is analyzed by distorted wave born approximation method. The experimental data of the elastic scattering angular distributions could be described reasonably well by the optical model at forward angles; however, anomalous large-angle scattering is observed in the angular distributions of both the elastic and inelastic channels for all measured energies. Elastic and inelastic scatterings are investigated using the coupled reaction channel method. The elastic and inelastic scattering, transfer reactions for the ground and excited states, and their coupling effects are considered in the coupled reaction channel scheme. In addition, the influence of the breakup effects of the weakly bound ^{6}Li and ^{7}Li is investigated by including three resonance states of ^{6}Li and two resonance states of ^{7}Li in the coupled reaction channel framework. The observed anomalous large-angle scattering is explained using the transfer reaction mechanism and breakup effect, and the calculated results reproduce the experimental data reasonably well.

Keywords: Anomalous large-angle scattering, Coupled reaction channel, Transfer reaction, Breakup effect

I. INTRODUCTION

Early investigations on collisions between nuclei with similar masses have indicated that the reaction mechanisms involved are intricate, and the angular distributions of elastic and inelastic scattering exhibit obvious anomalous large-angle scattering (ALAS) [1–6]. The optical model (OM) is an important theoretical model of nuclear reaction analysis. It has been widely used to investigate elastic scattering processes and has achieved significant success in calculations and analyses of experimental data [7–9]. However, the description of elastic scattering between nuclei with similar masses using OM alone is inadequate [10–15]. The experimental data show an obvious enhancement in the elastic scattering angular distributions at intermediate and backward angles. This behavior is typically observed in systems where projectiles and targets share the same core structure [16–20], where the backward angles in the elastic scattering correspond to the forward angles in the transfer process. It is found that the ALAS is a result of specific reaction mechanisms in different reaction systems. For example, the elastic scattering angular distributions of the ^{9}Be+^{12}C system in the energy range $\mathrm{E_{lab}}(^{9}\mathrm{Be}) = 13.00 - 21.00\,\mathrm{MeV}$ were analyzed using OM and the distorted wave born approximation (DWBA) method [4]. This indicates the significance of the ^{3}He transfer process at intermediate and backward angles. For nα-type systems, where both the projectile and target consist of integer multiples of α particles, such as ^{16}O+^{24}Mg, ^{16}O+^{28}Si, and ^{12}C+^{24}Mg, the reactions have large α-spectroscopic factors. Therefore, the ALAS behavior is usually attributed to the α transfer process such as in Ref. [3, 21]. However, the spin reorientations of ^{11}B and ^{14}N dominate at intermediate and backward angles in the elastic scattering angular distributions of the ^{11}B+^{14}N system at $\mathrm{E_{lab}}(^{14}\mathrm{N}) = 88\,\mathrm{MeV}$ in Ref. [22]. In addition, the spin reorientation of ^{9}Be dominates at intermediate and backward angles where transfer reaction makes only a small contribution in the elastic scattering angular distribution of the ^{9}Be+^{15}N system at $\mathrm{E_{lab}}(^{15}\mathrm{N}) = 84\,\mathrm{MeV}$ as shown in Ref. [8]. The elastic scattering angular distributions of ^{11}B+^{12}C system in a broad energy range $\mathrm{E_{cm}}(^{11}\mathrm{B}) = 5.00 - 52.00\,\mathrm{MeV}$ were analyzed by the OM and the coupled reaction channels (CRC) method [20], which indicates that the potential scattering dominates at forward angles, the proton transfer process dominates at backward angles, and both these processes and spin reorientation of ^{11}B play important roles at the intermediate angular range. Therefore, various reaction mechanisms may lead to ALAS formation in different reaction systems. Exploring the origin of ALAS allows us to understand nuclear reaction mechanisms more clearly. If the incident projectile and target are both weakly bound light nuclei, another reaction mechanism termed breakup effect, may have a high probability of occurrence, which has been of interest to both experimental and theoretical nuclear physicists [23, 24].

^{6}Li+^{7}Li system is a good prototype of nuclear reactions between adjacent weakly bound light nuclei, which can be conceptualized as comprising two identical ^{6}Li cores accompanied by a neutron bound to one of these cores, i.e. assuming that ^{7}Li exhibits a n+^{6}Li cluster structure when considering n-transfer processes. The interchange of these identical cores in such a configuration has a considerable probability, which will lead to the notable involvement of neutron transfer in both elastic and inelastic scatterings. Additionally, ^{6}Li and ^{7}Li are weakly bound nuclei that break easily into α+d and α+t, respectively. The breakup effect can affect the scattering channels [25–37]. Therefore, the transfer reaction and

* This work was supported by the President's Fund of China Academy of Engineering Physics (YZJJZQ2023022) and Nature Science Foundation of Shanxi Province, China (No.202103021224309 and No.201901D111317)

† Corresponding author, guo_hairui@iapcm.ac.cn

breakup effect must be considered in the analysis of ^{6}Li+^{7}Li scattering, and the spin reorientation also be considered according to previous studies [20, 22]. Pottvast et al. presented experimental data [38] on the elastic and inelastic scattering angular distributions of the ^{6}Li+^{7}Li reaction for the first time to study the reaction mechanism of scattering in asymmetric systems. They employed the OM and DWBA methods to calculate the angular distributions of ^{6}Li elastic scattering and inelastic scattering to the first excited state of ^{7}Li, taking into account the transfer reaction mechanism. However, their results underestimated the experimental data in the ALAS region. Xu et al. [39] employed the OM and DWBA methods to calculate the ^{6}Li elastic scattering angular distributions and the inelastic scattering to the first excited state of 1p-shell nuclei; the calculated results of the elastic scattering angular distributions were in reasonable agreement with the experimental data at forward angles, whereas large discrepancies were observed at backward angles.

The purpose of this study is to investigate the reaction mechanism of ^{6}Li+^{7}Li scattering and analyze the angular distributions for both elastic and inelastic scatterings at energies $\mathrm{E_{lab}}$=10−40 MeV. The CRC method is employed in the analysis, and the elastic and inelastic scatterings, ground- and excited-state transfer reaction channels, and their coupling effects are considered. The São Paulo potential obtained using a double-folding model for the ^{6}Li+^{7}Li system is used as a "bare" potential. Therefore, it is a suitable potential for investigating the coupling effects within the CRC method.

The remainder of this paper is organized as follows. Section II outlines the method and theoretical formalism. In Section III, the calculation results and discussion are presented. Finally, a brief summary and conclusions are presented in Section IV.

II. PROPOSED METHOD AND THEORETICAL FORMALISM

To understand the reaction mechanism, ^{6}Li+^{7}Li scattering is analyzed in the three frameworks. First, routine spherical nucleus OM and DWBA methods are employed to calculate the elastic scattering and inelastic scattering of the first excited state of ^{7}Li, respectively. Second, the CRC method is used with consideration of elastic scattering ^{7}Li(^{6}Li,^{6}Li)^{7}Li, inelastic scattering ^{7}Li(^{6}Li,^{6}Li)^{7}Li$_{0.48}$, single neutron ground-state transfer ^{7}Li(^{6}Li,^{7}Li$_{\mathrm{gs}}$)^{6}Li and single neutron excited-state transfer ^{7}Li(^{6}Li,^{7}Li$_{0.48}$)^{6}Li channels. Third, excluding the four reaction channels, three resonance states of ^{6}Li at excited energies of 2.186 MeV (3^{+}), 4.312 MeV (2^{+}), and 5.65 MeV (1^{+}), as well as two resonance states of ^{7}Li at excited energies of 4.63 MeV (3.5^{-}) and 6.68 MeV (2.5^{-}) are included in the CRC calculation. This is to investigate the approximate influence of the breakup effect, since it is found that the D-wave resonance channels among the ^{6}Li breakup channels and the F-wave resonance channels among the ^{7}Li breakup channels are significant in couplings to the elastic channel[35, 36]. The calculations are performed using the FRESCO code [40], which considers finite-range transfer and the full complex remnant, and uses the same interaction potential for the initial and final channels.

In the spherical-nucleus OM, the nucleus is assumed to be spherical. Only the shaped elastic scattering channel is highlighted, and the influences of all other channels are expressed as equivalent effects. The spherical-nucleus OM is a typical tool for the analysis of the nucleus-nucleus elastic scattering process. The stationary state Schrödinger equation of the system is defined as follows:

$$(E - T_\alpha - U_\alpha(R))\Psi_\alpha(R) = 0 \tag{1}$$

where the subscript α denotes the incident channel, E denotes the total energy of the system, T_α denotes the relative kinetic energy of the system, $U_\alpha(R)$ denotes the optical model potential between the projectile and the target nucleus, $\Psi_\alpha(R)$ denotes the wave function of the system, and R denotes the distance between the projectile and the target nucleus.

The incident particle moves under the action of the mean field, causing direct reactions owing to residual interactions. When the residual interaction is weak, particularly for spherical nuclei near the full shell, it is appropriate to employ DWBA method for direct reaction calculations. The corresponding equations are defined as follows:

$$(E - E_\alpha - T_\alpha - U_\alpha(R))\Psi_\alpha(R) = V_\beta(R,\xi_\alpha)\Psi_\beta(R) \tag{2}$$

where the subscript β indicates the outgoing channel, E_α denotes the excitation energy of the target nucleus, $V_\beta(R,\xi_\alpha)$ denotes the residual interaction term between the projectile and target nucleus.

When the residual interaction is strong, the coupling effect cannot be neglected. Therefore, it is appropriate to employ CRC method for direct reaction calculations. The CRC equations are as follows:

$$(E - E_\alpha - T_\alpha - U_\alpha(R))\Psi_\alpha(R) = \sum_{\alpha\neq\beta} V_\beta(R)\Psi_\beta(R) \tag{3}$$

where $V_\beta(R) = \int \phi^*(\xi_\alpha)(V_\alpha(\vec{R}) - U_\alpha(R))\phi(\xi_\beta)d\Omega d\xi$, $V_\alpha(\vec{R})$ denotes interaction potential between the projectile and the target nucleus, $\phi(\xi_\alpha)$ and $\phi(\xi_\beta)$ are the internal wave functions corresponding to the incident channel and outgoing channel, respectively. The channel-channel coupling effects are explicitly included in the CRC method.

The elastic scattering and elastic transfer processes are experimentally indistinguishable, hence both ^{7}Li(^{6}Li,^{6}Li)^{7}Li and ^{7}Li(^{6}Li,^{7}Li$_{\mathrm{gs}}$)^{6}Li processes must be considered to obtain the elastic scattering angular distribution, and the same is true for ^{7}Li(^{6}Li,^{6}Li)^{7}Li$_{0.48}$ and ^{7}Li(^{6}Li,^{7}Li$_{0.48}$)^{6}Li to obtain the inelastic scattering angular distribution [6, 41]. To consider the interference between elastic scattering and elastic transfer in the theoretical calculation, the elastic transfer amplitude $f_{\mathrm{eltr}}(\pi - \theta_{\mathrm{c.m.}})$ must be added to the elastic scattering amplitude $f_{\mathrm{el}}(\theta_{\mathrm{c.m.}})$. The same is true when considering the interference between inelastic scattering amplitude $f_{\mathrm{inel}}(\theta_{\mathrm{c.m.}})$ and inelastic transfer amplitude $f_{\mathrm{inltr}}(\pi - \theta_{\mathrm{c.m.}})$ in the theoretical calculation. Subsequently, the elastic scattering angular distribution and the inelastic scattering angular

distribution is expressed as follows:

$$\frac{d\sigma}{d\Omega}(\theta_{\rm c.m.}) = \frac{1}{(2J_{p,(p')}+1)(2J_{t,(t')}+1)} \cdot \sum_{m'M'mM} |f_{\rm el(inl)}(\theta_{\rm c.m.}) + f_{\rm eltr(inltr)}(\pi-\theta_{\rm c.m.})|^2 \quad (4)$$

where J_p, $J_{p'}$, J_t and $J_{t'}$ are the state spins for the projectile ground, projectile excited, target ground, and the target excited, respectively.

The latest version of the São Paulo potential (SPP2) [42] is used to describe the optical model potential of the ^{6}Li+^{7}Li system as input to the Fresco code, and is written as follows:

$$V_{\rm OP}^{\rm SPP2}(R) = (N_r + iN_i)V_F(R) \quad (5)$$

where N_r and N_i are the normalization coefficients, taken as 1 and 0.8, respectively, as suggested in Refs. [43, 44]. The folding potential $V_F(\vec{R})$ depends on the matter density in the following form:

$$V_F(R) = \int \rho_{m1}(\vec{r_1})\rho_{m2}(\vec{r_2})v_{mm}(\vec{R}-\vec{r_1}+\vec{r_2})d\vec{r_1}d\vec{r_2} \quad (6)$$

where $\rho_{m1}(\vec{r_1})$ and $\rho_{m2}(\vec{r_2})$ are the matter densities of the two colliding nuclei, which are the experimental density for ^{6}Li and the theoretical Dirac-Hartree-Bogoliubov density for ^{7}Li, respectively, obtained from Ref. [42]. v_{mm} is an effective nucleon-nucleon interaction with a Gaussian distribution given by

$$v_{mm}(\vec{r}) = -U_0 e^{-(r/a)^2} e^{-4\nu^2/c^2} \quad (7)$$

where the values of U_0 and a are 735.813 MeV and 0.5 fm, respectively; c represents the speed of light; and ν denotes the relative velocity between the interacting nuclei.

The velocity is related to the kinetic energy as follows:

$$E_K(R, E_{\rm c.m.}) = E_{\rm c.m.} - V_C(R) - V_F(R) \quad (8)$$

through the following relativistic expression:

$$\nu^2(R, E_{\rm c.m.}/c^2) = 1 - (\frac{\mu c^2}{\mu c^2 + E_K})^2 \quad (9)$$

V_C denotes the Coulomb potential, and μ denotes the reduced mass of the system.

To investigate the influence of the coupling effect on the scattering channels, the CRC method is used. The inelastic excitations of ^{6}Li and ^{7}Li are described by using a rotational model. Such collective motions can be described in terms of permanent deformations of the nuclear shape with deformation lengths δ_λ. The interaction to which an incident particle is subjected is described by a nonspherical optical-model potential. Because axisymmetric deformation is considered, the deformed nuclear shapes can be expressed as follows:

$$R(\theta', \varphi') = R_0[1 + \sum_\lambda \beta_\lambda Y_{\lambda 0}(\theta', \varphi')] \quad (10)$$

where R_0 denotes the spherical nucleus radius equal to $r_0 A^{\frac{1}{3}}$, $Y_{\lambda 0}$ denotes the spherical harmonics, β denotes the multipolarity deformation parameter of the nucleus, λ denotes the multipolarity of the transition, θ' and φ' are angular coordinates in the body-fixed system.

The deformation potential felt by the incident particle can be expressed as follows:

$$V(\boldsymbol{\xi}, \boldsymbol{R}) = U(R - \Delta(\hat{\boldsymbol{R}}, \boldsymbol{\xi})) \quad (11)$$

where $U(R)$ denotes the OM potential to be deformed using deformation lengths δ_λ of the multipole λ and the 'shift function' has the multipole expansion

$$\Delta(\boldsymbol{R}') = \sum_{\lambda\neq 0} \delta_\lambda Y_\lambda^0(\boldsymbol{R}') \quad (12)$$

where $\hat{\boldsymbol{R}}'$ denotes the vector $\hat{\boldsymbol{R}}$ in the body-centered frame of coordinates defined by $\boldsymbol{\xi}$.

The abovementioned deformation potential $V(\boldsymbol{\xi}, \boldsymbol{R})$ can be expanded by the spherical harmonic function in the body-fixed coordinate system. Subsequently, the body-fixed coordinate system is projected to space-fixed coordinate system through the rotational function D. Therefore, the optical model potential of the deformed nucleus in the space-fixed system coordinates can be obtained as follows:

$$V(\boldsymbol{\xi}, \boldsymbol{R}) = \sum_{\lambda\mu} V_\lambda(R) D^\lambda_{\mu 0}(\alpha, \beta, \gamma) Y_{\lambda\mu}(\theta, \varphi) \quad (13)$$

where α, β, γ are the Euler coordinates; θ and φ are the angular coordinates in the space-fixed system; $V_\lambda(R)$ is unrelated to the angular coordinates and can be expressed as follows:

$$V_\lambda(R) = \frac{1}{2}\int_{-1}^{1} U(r(R, cos\theta))Y_\lambda^\mu(\theta, 0)d(cos\theta) \quad (14)$$

and

$$r(R, cos\theta) = R - \sqrt{\frac{2\lambda+1}{4\pi}} P_\lambda(\theta)\delta_\lambda + \sum_\lambda \frac{\delta_\lambda^2}{4\pi R_U} \quad (15)$$

where R_U is the average potential radius.

When the deformation lengths δ_λ are small, the form factors $V_\lambda(R)$ are simply the first derivatives of the $U(R)$ function as follows [40].

$$V_\lambda(R) = -\frac{\delta_\lambda}{\sqrt{4\pi}}\frac{dU(R)}{dR}, \quad (16)$$

with the same shape for all the multipoles $\lambda > 0$.

The ground-state reorientation and excited-state reorientation notated by $< I^\pi_{\rm gs}K_{\rm gs}|V(\boldsymbol{\xi}, \boldsymbol{R})|I^\pi_{\rm gs}K_{\rm gs} >$ and $< I^\pi_{\rm ex}K_{\rm ex}|V(\boldsymbol{\xi}, \boldsymbol{R})|I^\pi_{\rm ex}K_{\rm ex} >$, as well as the transitions from the ground state to excited state of the ^{6}Li and ^{7}Li notated by $< I^\pi_{\rm ex}K_{\rm ex}|V(\boldsymbol{\xi}, \boldsymbol{R})|I^\pi_{\rm gs}K_{\rm gs} >$ is calculated using the CRC method. In the abovementioned transition matrices, $|I^\pi_{\rm gs}K_{\rm gs}>$ and $|I^\pi_{\rm ex}K_{\rm ex}>$ represent the ground- and excited-state wave functions respectively, with spins $I_{\rm gs}$, $I_{\rm ex}$ and their

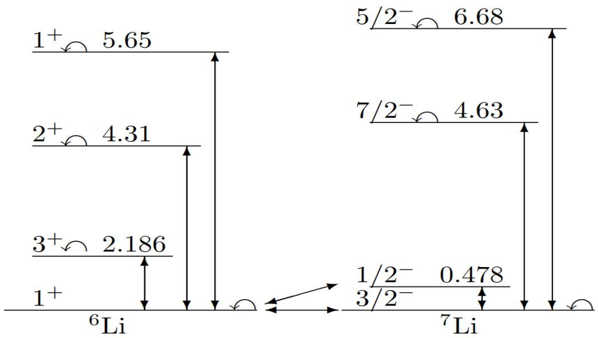

Fig. 1: (Color online) Coupling schemes for the transitions to the excited states of ^{6}Li and ^{7}Li, the transitions of the ^{6}Li and ^{7}Li spin reorientations are marked with arc arrows.

projections $K_{\rm gs}$, $K_{\rm ex}$ onto the intrinsic symmetry axes. The transitions to these states are calculated using the form factors.

The following reduced deformation length

$$\Delta_\lambda(I\to I_{\rm ex}) =(-1)^{(I-I_{\rm ex}+|I-I_{\rm ex}|)/2} \cdot \sqrt{2I+1}\delta_\lambda < IK\lambda 0|I_{\rm ex}K > \tag{17}$$

is used in the rotational model for CRC calculations. The quadrupole deformation lengths of ^{6}Li, denoted by δ_2^{ij}, reflect the transition from the initial state i to the final state j in a rotational nucleus with bandhead K and can be derived from the reduced electric-quadrupole transition probability B(E2):

$$\sqrt{B(E2;KJ_i\to KJ_j)} =| < J_iK20|J_jK > \cdot \frac{Ze}{A}\int_0^\infty \rho_2^{ij}(r)r^4dr| \tag{18}$$

where $\rho_2^{ij}(r)$ denotes the quadrupole transition density, expressed as

$$\rho_2^{ij}(r) = -\delta_2^{ij}\frac{d\rho_0(r)}{dr} \tag{19}$$

$\rho_0(r)$ denotes the ground-state charge density of the nucleus, which can be found in Ref. [1].

The ^{6}Li+^{7}Li elastic and inelastic scattering channels, single neutron transfer reaction channel and breakup effect are included in the coupled reaction channel scheme, as shown in Fig. 1. The spin reorientations of ^{6}Li and ^{7}Li in the ground and excited states are also included in the CRC calculations. The reorientation quadrupole deformation length, denoted by δ_2^{ii} in (19), for the ground and excited states of ^{6}Li and ^{7}Li are 1.000 fm and 2.000 fm, respectively.

The reduced transition probabilities B(E_2) between the ground state and the 2.186 MeV, 4.312 and 5.650 MeV resonances were obtained from Ref. [45]. The deformation parameters are presented in Table 1.

The neutron transfers to the ^{6}Li forming the ground, and the first excited states of ^{7}Li are included in the CRC calculations. The bound-state wave functions of ϕ(n + ^{6}Li), dependent on the internal coordinates, are obtained by solving the Schrödinger equation using a real Woods-Saxon potential with radius parameters $R = 3.24$ fm and diffuseness $a = 0.65$ fm. The potential depth $V(\mathrm{n} + {}^6\mathrm{Li})$ is adjusted to reproduce the binding energies of the ^{7}Li ground state $E_{\rm bind}$=7.25 MeV and the first excited state $E_{\rm bind}$=6.77 MeV. The number of nodes in the bound-state wave function is obtained based on the Wildermuth condition: $2N + L = \sum_{i=1}^{1}(2n_i + l_i)$, where N and L represent the number of nodes and the angular momentum of the nucleons respectively, and n_i and l_i are the quantum numbers associated with the Fermi levels $(0p_{3/2})$ and $(0p_{1/2})$ occupied by nucleons in ^{7}Li [3]. It should be noted that the number of nodes defined in the FRESCO code contains the origin; therefore, the number of nodes should be n+1 when calculating using the FRESCO code. The spectroscopic amplitudes $S^{1/2}_{\langle ^7\mathrm{Li_{g.s.}}|^6\mathrm{Li_{g.s.}}\rangle}$ and $S^{1/2}_{\langle ^7\mathrm{Li_{0.48}}|^6\mathrm{Li_{g.s.}}\rangle}$ are taken from Ref. [38].

TABLE 1: Transition multipolarity and deformation parameters.

Nuclei	$E_{\rm ex}$(MeV)	j^π	λ	Δ_λ(fm)	Ref.
^{6}Li	0.000	1.0^+	2	−1.095	
	2.186	3.0^+	2	3.358	[45]
	4.312	2.0^+	2	2.207	[45]
	5.650	1.0^+	2	1.315	[45]
^{7}Li	0.000	1.5^-	2	−1.800	
	0.478	0.5^-	2	2.800	[38]
	4.630	3.5^-	2	2.869	[46]
	6.680	2.5^-	2	1.171	[46]

III. RESULTS AND DISCUSSION

First, the angular distributions of ^{6}Li elastic scattering and inelastic scattering to the first excited state of ^{7}Li at incident energies from 10.0 MeV to 40.0 MeV were calculated using the traditional OM and DWBA methods, respectively. The calculated results are shown in Figs. 3 (a-g) and Figs. 4 (a-g) using the solid curves named OM and DWBA, respectively. In Figs. 3 (a-g), the calculated results of the elastic scattering angular distributions are in reasonable agreement with the experimental data at forward angles, whereas large discrepancies were observed at backward angles. A similar situation occurred for the inelastic scattering angular distributions, as shown in Figs. 4 (a-g). Therefore, the contributions of other reaction mechanisms to elastic and inelastic scatterings must be considered to describe ALAS, and the CRC method is used for this purpose.

Next, the CRC calculation is performed by coupling the elastic scattering ^{7}Li(^{6}Li,^{6}Li)^{7}Li, inelastic scattering ^{7}Li(^{6}Li,^{6}Li)^{7}Li$_{0.48}$, single neutron ground-state transfer ^{7}Li(^{6}Li,^{7}Li$_{\rm gs}$)^{6}Li, and single neutron excited-state transfer ^{7}Li(^{6}Li,^{7}Li$_{0.48}$)^{6}Li channels to explain the ALAS. The cal-

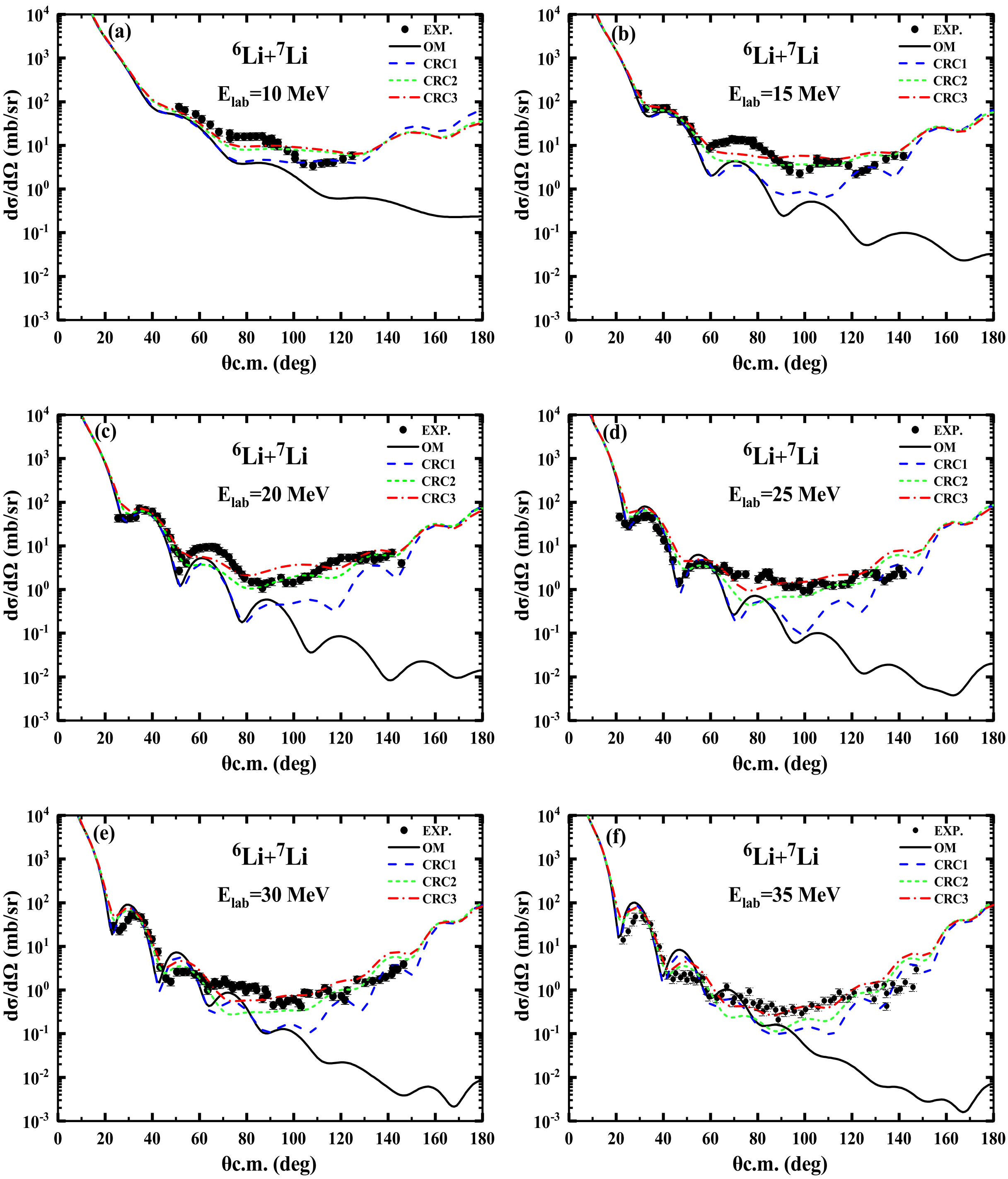

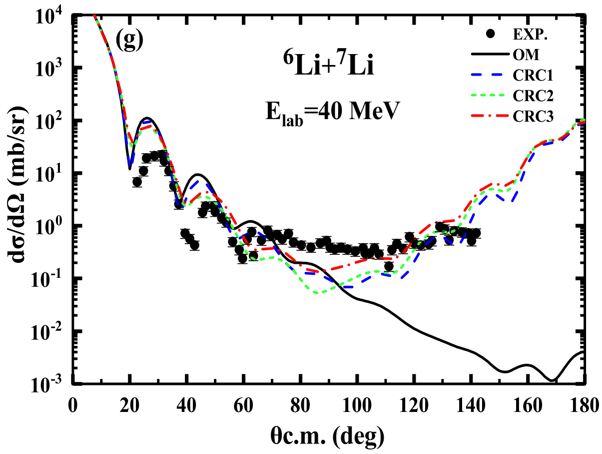

Fig. 2: Comparisons of the calculated elastic scattering angular distributions with the experimental data [38] at energies $E_{lab}(^6Li)$=10-40 MeV. The solid, dashed, short-dashed and dash-dotted curves present the OM, CRC1, CRC2 and CRC3 results, respectively. Details of the calculations are described in the text. (**a**) $E_{lab}(^6Li)$ = 10 MeV, (**b**) $E_{lab}(^6Li)$ = 15 MeV, (**c**) $E_{lab}(^6Li)$ = 20 MeV, (**d**) $E_{lab}(^6Li)$ = 25 MeV, (**e**) $E_{lab}(^6Li)$ = 30 MeV, (**f**) $E_{lab}(^6Li)$ = 35 MeV, (**g**) $E_{lab}(^6Li)$ = 40 MeV.

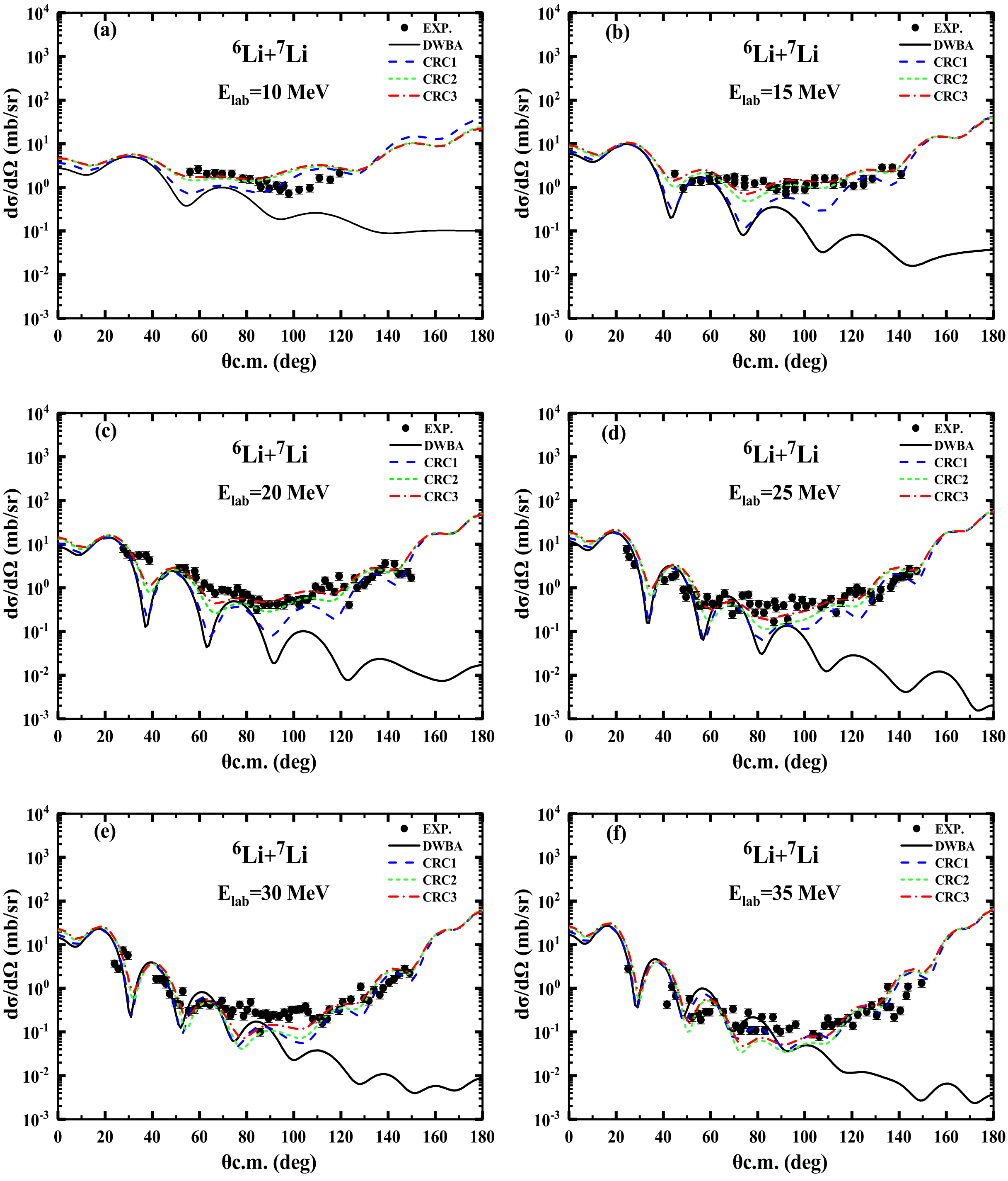

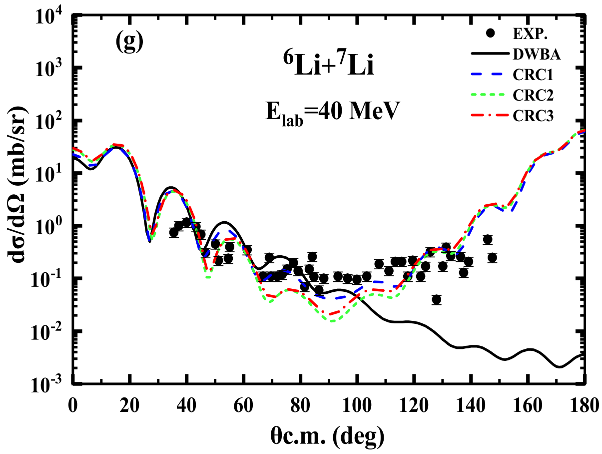

Fig. 3: (Color online) Comparisons of the calculated inelastic scattering angular distributions with the experimental data [38] at energies $E_{lab}(^6Li) = 10$-40 MeV. The solid, dashed, short-dashed and dash-dotted curves depict the DWBA, CRC1, CRC2 and CRC3 results, respectively. Details of the calculations are described in the text. (a) $E_{lab}(^6Li)$ = 10 MeV, (b) $E_{lab}(^6Li)$ = 15 MeV, (c) $E_{lab}(^6Li)$ = 20 MeV, (d) $E_{lab}(^6Li)$ = 25 MeV, (e) $E_{lab}(^6Li)$ = 30 MeV, (f) $E_{lab}(^6Li)$ = 35 MeV, (g) $E_{lab}(^6Li)$ = 40 MeV.

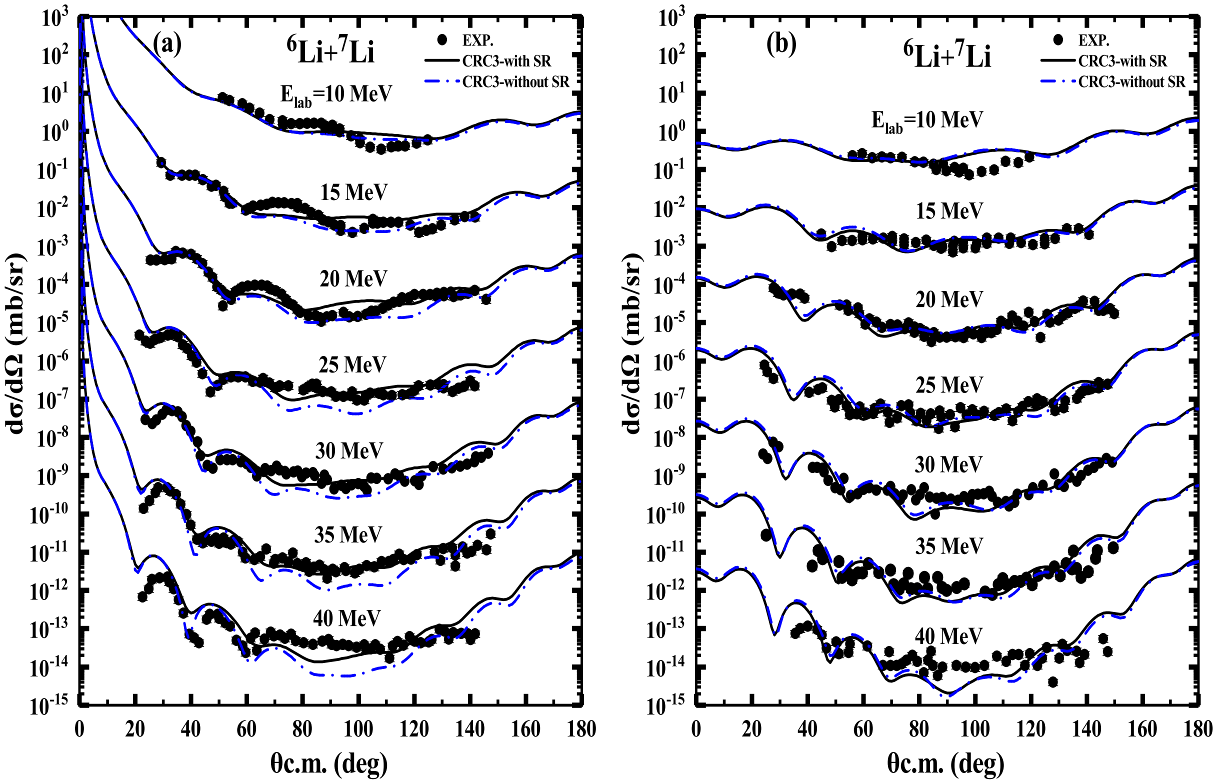

Fig. 4: (Color online) Comparisons of the calculated results with the experimental data at energies $E_{lab}(^6\mathrm{Li})$ = 10-40 MeV.The solid and dash-dotted curves present the results with and without spin reorientations respectively, based on CRC3 scheme. (a) Elastic scattering angular distribution, (b) Inelastic scattering angular distribution.

culated results of the elastic scattering and inelastic scattering angular distributions at incident energies from 10.0 MeV to 40.0 MeV are shown by dashed curves named CRC1 in Figs. 3 (a-g) and Figs. 4 (a-g). Overall, the calculated results were significantly better than the OM and DWBA results. It can be concluded that the transfer reaction mechanism plays a significant role at large angles in elastic and inelastic scattering; however, some of the results are still unsatisfactory. To describe the experimental data better, other reaction mechanisms must be considered.

Finally, the breakup effect was also considered in CRC calculations. Specifically, the coupling reaction framework incorporated contributions from the three resonance states of ^{6}Li at excitation energies of 2.186 MeV (3^+), 4.312 MeV (2^+), and 5.65 MeV (1^+), as well as two resonance states of ^{7}Li at excited energies of 4.63 MeV (3.5^-) and 6.68 MeV (2.5^-) to investigate the effect of breakup. Based on the four reaction channels of CRC1 scheme, the contributions of the three resonance states of ^{6}Li were first added to the coupling channel scheme, and the calculated results are shown by the short-dashed curves named CRC2 in Figs. 3 (a-g) and Figs. 4 (a-g). The results are better than those of the CRC1 scheme, which highlights the importance of the ^{6}Li breakup effect. However, the calculated results underestimate the experimental data over a broad angular range. Then, based on the CRC2 scheme, the contribution of the two resonance states of ^{7}Li is added to the coupling channel scheme, and the calculated results are shown by the dashed–dotted curves named CRC3 in Figs. 3 (a-g) and Figs. 4 (a-g). The results are further improved compared to the CRC2 scheme and provide a reasonable description of the experimental data over the entire angle range. This demonstrates that the breakup effects of ^{6}Li and ^{7}Li yield non-negligible contributions at intermediate and backward angles.

To investigate the influence of spin reorientations of the ^{6}Li and ^{7}Li, the elastic scattering and inelastic scattering angular distributions are calculated with and without the spin reorientations in the CRC3 scheme, and the results are compared in Fig. 5. The results considering spin reorientation are slightly better, indicating that spin reorientation plays a non-negligible role in the ^{6}Li + ^{7}Li scattering system.

The São Paulo potential is obtained by the double-folding model, which is a bare potential and only gives the real part of the interaction potential; the imaginary part is assumed to be proportional to the real part of the São Paulo potential through the normalization factor Ni. In the calculations above, 0.8 is adopted as the normalization factor, which is the average value for the analyses of different nuclear scattering systems in Refs. [43, 44]. Different normalization factor values are discussed. The calculated results with Ni=0.8, Ni=1.0 and Ni=0.6 are shown by the solid, dashed, and dash-dotted curves, respectively, in Fig. 6. In general, the results calcu-

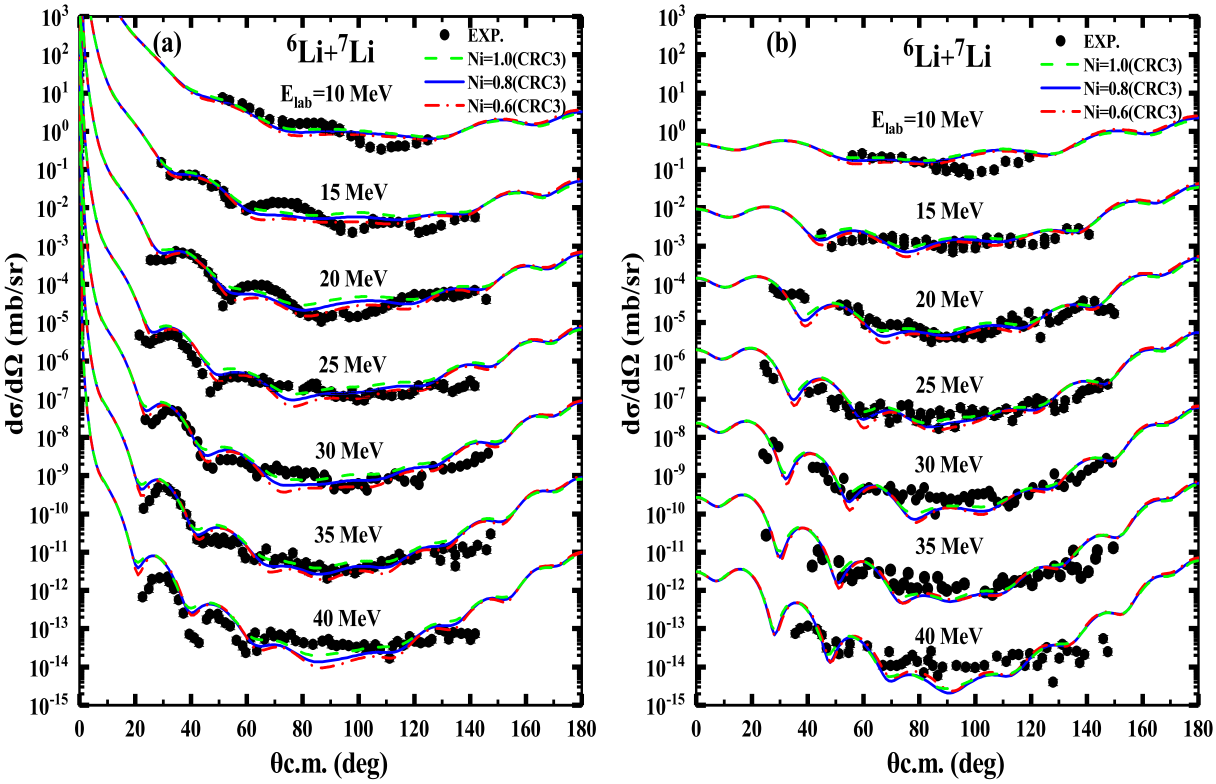

Fig. 5: (Color online) Comparisons of the calculated results with the experimental data at energies $E_{lab}(^6Li)$ = 10-40 MeV.The solid, dashed, and dash-dotted curves present the results with Ni=0.8, Ni=1.0 and Ni=0.6 respectively, based on CRC3 scheme. (a) Elastic scattering angular distribution, (b) Inelastic scattering angular distribution.

lated with Ni=0.8 are slightly better than the others. Therefore, Ni=0.8 is appropriate for the present analysis.

In addition, a comparative analysis of the angular distributions of both elastic and inelastic scatterings at $E_{lab}(^6Li) = 35$ MeV is conducted with the previous work [38] which considered only the potential scattering, inelastic scattering and transfer processes using OM and DWBA methods as shown in Fig. 7 a and Fig. 7 b. The present results can reasonably reproduce the experimental data at large angles $\theta_{c.m.} > 60°$; however, the previous work could not. This indicates that the breakup and coupling mechanisms are important in the ^{6}Li+^{7}Li scattering processes.

To further investigate the influence of the breakup effects of ^{6}Li and ^{7}Li, the elastic scattering and inelastic scattering angular distributions were calculated again in the CRC3 scheme with the ^{6}Li–^{7}Li optical potential replaced by the phenomenological optical potential V-GL-4 given in Ref. [38]. The calculated results are indicated by dashed curves, named CRC3-POP, in Fig. 8. These results are better than those reported in Ref. [38] denoted by the solid curves, highlighting the importance of the breakup effect. If the spectroscopic amplitude of the $(0p_{3/2})$ state of $^7Li_{gs}$ is adjusted from 0.657 to 1.0, the calculated results, denoted by the dash-dotted curves in Fig. 8 better matches the experimental data.

Based on the above analyses, it can be concluded that potential scattering dominates at forward angles where the transfer reaction and breakup effect makes a small contribution, whereas transfer reaction and breakup effects contribute significantly at middle and large angles for both the elastic and inelastic scatterings of the ^{6}Li+^{7}Li system. The spin reorientations of ^{6}Li and ^{7}Li provide non-negligible contributions at intermediate and backward angles.

IV. SUMMARY AND CONCLUSION

The angular distributions of a ^{6}Li+^{7}Li elastic and inelastic scatterings were analyzed in three frameworks. The SPP2 potential provides a reasonable description of ^{6}Li+^{7}Li elastic scattering angular distributions at forward angles $\theta_{c.m.} < 60°$ in the energy range $E_{lab} = 10$-40 MeV. ALAS was explained using CRC method that considers the elastic and inelastic scattering reaction channels, spin reorientations of ^{6}Li and ^{7}Li, ground-state transfer, and excited-state transfer reaction channels. Three resonance states of ^{6}Li and two resonance states of ^{7}Li were included to approximately consider the breakup effect. The The calculated results provide a reasonable description of the experimental data over the entire angle range at incident energies of $10.0\,\mathrm{MeV}$ to $40.0\,\mathrm{MeV}$. Moreover, compared with previous works, the present work provides a better description of the experimental data. It was concluded that the transfer and breakup mechanisms are crit-

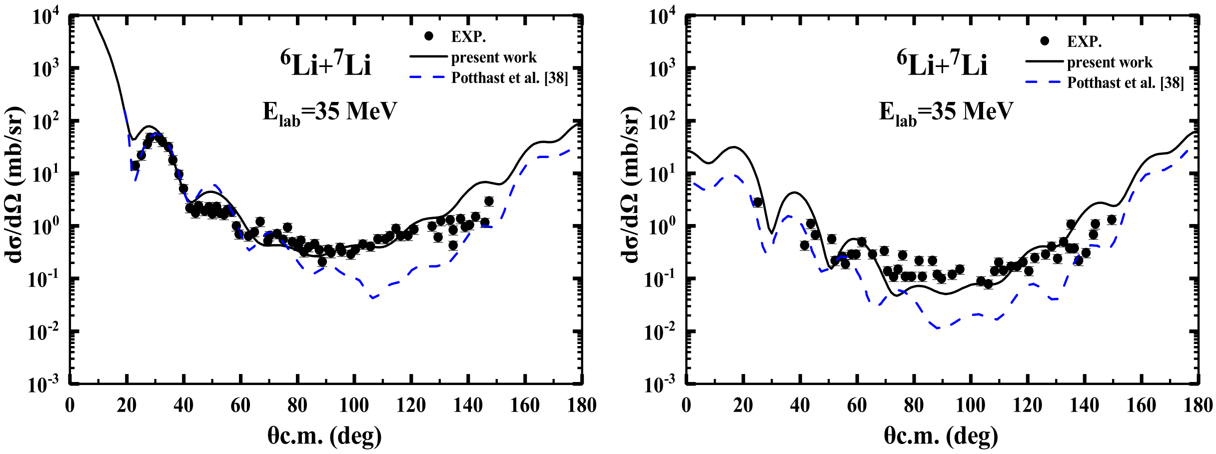

(a) (b)

Fig. 6: (Color online) Comparisons of present calculated results (solid lines) with those given by Ref. [38] (dashed lines) and experimental data at $E_{lab}(^6Li)$ = 35 MeV. (*a*) Elastic scattering angular distribution, (*b*) Inelastic scattering angular distribution.

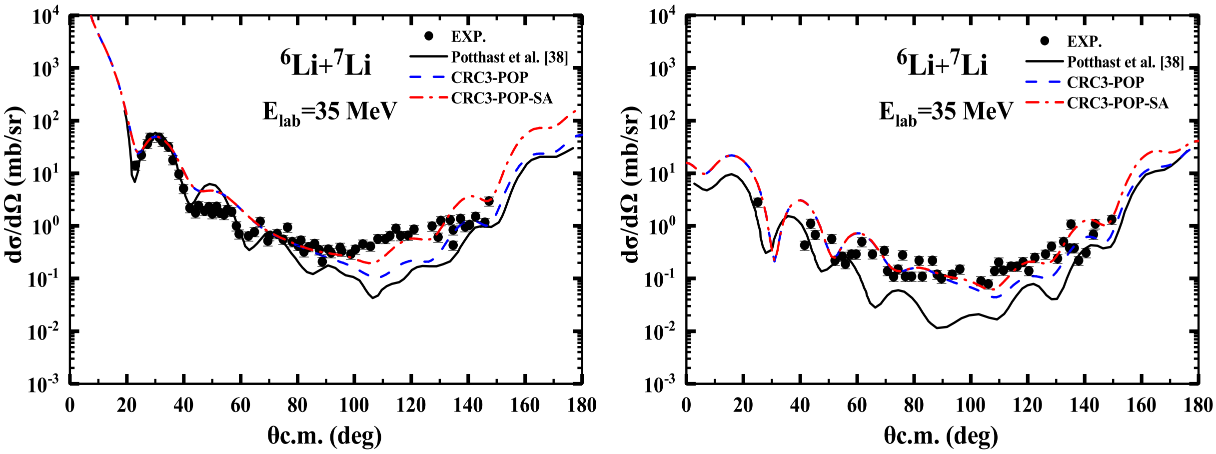

(a) (b)

Fig. 7: (Color online) Comparisons of the calculated results with the experimental data at $E_{lab}(^6Li)$ = 35 MeV.The solid, dashed, and dash-dotted curves present Potthast et al [38] results, the calculated results in the CRC3 scheme with phenomenological V-GL-4 potential, and with the spectroscopic amplitude of the (0p3/2) state of $^7Li_{gs}$ as 1.0, respectively. (*a*) Elastic scattering angular distribution, (*b*) Inelastic scattering angular distribution.

ically important in ^{6}Li+^{7}Li scattering, and the contributions of the ^{6}Li and ^{7}Li spin reorientations in the ground and excited states cannot be ignored. All of these reaction mechanisms should be considered in the study of nuclear reactions between adjacent weakly bound light nuclei.

---

[1] J. Carter, Z.Z. Vilakazi, R.W. Fearick et al., Elastic and inelastic scattering in the ^{6}Li, ^{9}Be + ^{12}C systems: excitation of unbound excited states and cluster transfers. Nucl. Phys. A **591**, 349–370 (1995). doi: 10.1016/0375-9474(95)00199-B

[2] A.T. Rudchik, O.A. Momotyuk, V.A. ZimanA et al., Energy dependence of the nucleus–nucleus interaction in the ^{9}Be + ^{12}C system and the ^{9}Be reorientation. Nucl. Phys. A **662**, 44–62 (2000). doi: 10.1016/S0375-9474(99)00369-3

[3] M.C. Morais, R. Lichtenthäler., α-Spectroscopic factor of $^{16}O_{gs}$ from the $^{12}C(^{16}O,^{12}C)^{16}O$ reaction. Nucl. Phys. A **857**, 1–8 (2011). doi: 10.1016/j.nuclphysa.2011.03.005

[4] R.A.N. Oliveira, N. Carlina, R. Liguori Neto et al., Study of ^{9}Be + ^{12}C elastic scattering at energies near the Coulomb barrier. Nucl. Phys. A **856**, 46–54 (2011). doi: 10.1016/j.nuclphysa.2011.02.005

[5] A.T. Rudchik, O.V. Herashchenko, K.W. Kemper et al., ^{15}N elastic and inelastic scattering by ^{11}B at 84 MeV. Nucl. Phys. A **939**, 1–12 (2015). doi: 10.1016/j.nuclphysa.2015.02.006

[6] D.Y. Pang, Y.L. Ye, D.X. Jiang et al., Elastic ^{3}He-transfer Reaction of ^{6}He on the ^{9}Be Target at 25 MeV/nucleon. AIP Conf. Proc. **865**, 16–21 (2006). doi: 10.1063/1.2398822

[7] Y.P. Xu, D.Y. Pang., Toward a systematic nucleus-nucleus potential for peripheral collisions. Phys. Rev. C **87**, 044605 (2013). doi: 10.1103/PhysRevC.87.044605

[8] A.T. Rudchik, K.A. Chercas, K.W. Kemper et al., Elastic and inelastic scattering of ^{15}N ions by ^{9}Be at 84 MeV. Nucl. Phys. A **947**, 161–172 (2016). doi: 10.1016/j.nuclphysa.2016.01.002

[9] Xinwu Su, Yinlu Han, Haiying Liang et al., Global phenomenological optical model potential for ^{8}Li projectile. Phys. Rev. C **95**, 054606 (2017). doi: 10.1016/j.nuclphysa.2007.03.004

[10] Yongli Xu, Yinlu Han, Jiaqi Hu et al., ^{6}Li global phenomenological optical model potential. Phys. Rev. C **98**, 024619 (2018). doi: 10.1103/PhysRevC.98.024619

[11] Yongli Xu, Yinlu Han, Jiaqi Hu et al., Global phenomenological optical model potential for the ^{7}Li projectile nucleus. Phys. Rev. C **97**, 014615 (2018). doi: 10.1103/PhysRevC.97.014615

[12] H. Takai, K. Koide, A. Bairrio Nuevo et al., Alpha-transfer contribution to ^{10}B + ^{14}N elastic scattering. Phys. Rev. C **38**, 741–747 (1988). doi: 10.1103/PhysRevC.38.741

[13] Yongli Xu, XinWu Su, Zhihao Sun et al., Description of elastic scattering for ^{7}Li-induced reactions on 1p-shell nuclei. Chin. Phys. C **48**, 024106 (2024). doi: 10.1088/1674-1137/ad1924

[14] A.T. Rudchik, Yu.O. Shyrma, K.W. Kemper et al. studied the elastic and inelastic scattering of ^{13}C + ^{18}O versus ^{12}C + ^{18}O and ^{13}C + ^{16}O. Nucl. Phys. A **852**, 1–14 (2011). doi: 10.1016/j.nuclphysa.2011.01.004

[15] S.Yu. Mezhevych, K. Rusek, A. T. Rudchik et al., ^{13}C + ^{11}B elastic and inelastic scattering and isotopic effects in ^{12,13}C + ^{11}B scattering. Nucl. Phys. A **724**, 29–46 (2003). doi: 10.1016/S0375-9474(03)01478-7

[16] L. JARCZYK, J. OKOLOWICZ, A. STRZAKOWSKI et al., LARGE ANGLE ELASTIC SCATTERING OF ^{9}Be IONS ON CARBON ISOTOPES. Nucl. Phys. A **316**, 139–145 (1979). doi: 10.1016/0375-9474(79)90676-6

[17] A. Barbadoro, F. Pellegrini, G. F. Segato et al., α-transfer contribution to ^{9}Be + ^{13}C elastic and inelastic scattering. Phys. Rev. C **41**, 2425–2428 (1990). doi: 10.1103/PhysRevC.41.2425

[18] J. F. Mateja, A. D. Frawley, P. B. Nagel et al., ^{12}C(^{9}Be, ^{9}Be)^{12}C(g.s., 4.43 MeV) reaction. Phys. Rev. C **20**, 176–182 (1979). doi: 10.1103/PhysRevC.20.176

[19] Guozhu He, Chengqun Gao and Pingzhi Ning, Alpha transfer process in ^{16}O+ ^{24}Mg elastic scattering. Phys. Rev. C **30**, 534–538 (1984). doi: 10.1103/PhysRevC.30.534

[20] A.T. Rudchik, A. Budzanowski, V.K. Chernievsky et al., The ^{11}B + ^{12}C elastic and inelastic scattering at E_{lab}(^{11}B=49 MeV) and energy dependence of the ^{11}B + ^{12}C interaction. Nucl. Phys. A **695**, 51–68 (2001). doi: 10.1016/S0375-9474(01)01106-X

[21] Jiayinghao Li, Zhihong Li, Youbao Wang et al., Nuclear astrophysics research based on HI-13 tandem accelerator. Nucl. Tech. 46, 080002 (2023).doi: 10.11889/j.0253-3219.2023.hjs.46.080002

[22] A.T. Rudchik, O.V. Herashchenko, K.W. Kemper et al., Elastic and inelastic scattering of ^{14}N ions by ^{11}B at 88 MeV versus that of ^{15}N + ^{11}B at 84 MeV. Nucl. Phys. A **941**, 167–178 (2015). doi: 10.1016/j.nuclphysa.2015.06.012

[23] Lei Yang, Chengjian Lin, Huiming Jia et al., Progress on nuclear reactions and related nuclear structure at low energies. Nucl. Tech. 46, 080006 (2023).doi: 10.11889/j.0253-3219.2023.hjs.46.080006

[24] Siyu Xu, Zhaoqing Feng., Cluster emission in massive transfer reactions based on dinuclear system model. Nucl. Tech. 46, 030501 (2023). doi: 10.11889/j.0253-3219.2023.hjs.46.030501

[25] J. Thompson, M.A. Nagarajan, Breakup Effects in the Elastic Scattering of ^{6}Li Ions. Phys. Lett. B **106** 163–166 (1981). doi: 10.1016/0370-2693(81)90899-6

[26] Yukinori SAKURAGI, Masanobu YAHIRO, Masayasu KAMIMURA, Projectile Breakup Effect on ^{6}Li Elastic Scattering from ^{28}Si and ^{31}Ca studied the microscopic coupled-channel method. Prog. Theor. Phys. **68**, 322–326 (1982). doi: 10.1143/ptp.68.322

[27] Hairui Guo, Yukinobu Watanabe, Takuma Matsumoto et al., Analysis of nucleon and triton emissions from nucleon- ^{7}Li collisions below 20 MeV. Phys. Rev. C **99**, 034602 (2019). doi: 10.1103/PhysRevC.99.034602

[28] Wendi Chen, Hairui Guo, Tao Ye et al., Application of the Lagrange-mesh method in continuum-discretized coupled-channel calculations. J. Phys. G Nucl. Partic. **49**, 075104 (2022). doi: 10.1088/1361-6471/ac7249

[29] Wendi Chen, Danyang Pang, Hairui Guo et al., Elastic scattering and total reaction cross sections of ^{6}Li examined via a microscopic continuum discretized coupled-channels model. Chin. Phys. C **48**, 014101 (2024). doi: 10.1088/1674-1137/ad0453

[30] Danyang Pang, R.S. Mackintosh et al., Dynamic polarization potential due to ^{6}Li breakup on ^{12}C. Phys. Rev. C **84**, 064611 (2011). doi: 10.1103/PhysRevC.84.064611

[31] Jin Lei, Antonio M. Moro, Comprehensive analysis of large α yields observed in ^{6}Li induced reactions. Phys. Rev. C **95**, 044605 (2017). doi: 10.1103/PhysRevC.95.044605

[32] N.C. Summers, F.M. Nunes, I.J. Thompson, Core transitions in the breakup of exotic nuclei. Phys. Rev. C **73**, 031603 (2006). doi: 10.1103/PhysRevC.73.031603

[33] Masayasu Kamimura, Masanobu Yahiro, Yasunori Iseri et al., Projectile Breakup Processes in Nuclear Reactions. Prog. Theor. Phys. Suppl. No **89**, 1–10 (1986). doi: 10.1143/PTPS.89.1

[34] Masanobu Yahiro, Kazuyuki Ogata, Takuma Matsumoto et al., The continuum discretized coupled-channels method and its applications. Prog. Theor. Phys. No **2012**, 01A206 (2012). doi: 10.1093/ptep/pts008

[35] Yukinori Sakuragi, Masanobu Yahiro, Masayasu Kamimura, Elastic Scattering and Breakup of ^{6}Li. Prog. Theor. Phys. No **70**, 1047 (1983). doi: 10.1143/PTP.70.1047

[36] Yukinori Sakuragi, Masanobu Yahiro, Masayasu Kamimura, Microscopic Coupled-Channels Study of Scattering and Breakup of Light Heavy-Ions. Prog. Theor. Phys. Suppl. No **89**, 136 (1986). doi: 10.1143/PTPS.89.136

[37] J.P. Fernández-García, M. Zadro, A. Di Pietro et al., Effects of coupling to breakup in the ^{6,7}Li + ^{64}Zn systems at near-barrier energies. Phys. Rev. C **92**, 054602 (2015). doi: 10.1103/PhysRevC.92.054602

[38] K.W. Potthast, H. Freiesleben, P. Rosenthal et al., Potential interaction and transfer in elastic ^{7}Li(^{6}Li, ^{6}Li) ^{7}Li and inelastic

^{7}Li(^{6}Li, ^{6}Li) ^{7}Li$_{0.48}$ scattering at E_{lab} = 9–40 MeV. Nucl. Phys. A **629**, 656–676 (1998). doi: 10.1016/S0375-9474(98)00651-4

[39] Yongli Xu, Xinwu Su, Yinlu Han et al., Optical potential for the elastic scattering of ^{6}Li projectile on 1p-shell nuclei. Int. J. Mod. Phys. E **31**, 2250093 (2022). doi: 10.1142/S0218301322500938

[40] I.J. Thompson, Coupled reaction channels calculations in nuclear physics. Comp. Phys. Rep. **7**, 167–212 (1988). doi: 10.1016/0167-7977(88)90005-6

[41] E.T. Li, Z.H. Li, Y.J. Li et al., Proton spectroscopic factor of the ^{12}C ground state from the ^{12}C(^{11}B,^{12}C)^{11}B elastic transfer reaction. Phys. Rev. C **90**, 067601 (2014). doi: 10.1103/PhysRevC.90.067601

[42] L.C. Chamon, B.V. Carlson, L.R. Gasques, São Paulo potential version 2 (SPP2) and Brazilian nuclear potential(BNP). Comp. Phys. Com. **267**, 108061 (2021). doi: 10.1016/j.cpc.2021.108061

[43] M.A.G. Alvarez, L.C. Chamon, M.S. Hussein et al., A parameter-free optical potential for the heavy-ion elastic scattering process. Nucl. Phys. A **723**, 93–103 (2003). doi: 10.1016/S0375-9474(03)01158-8

[44] M.A.G. Alvarez, N. Alamanos, L.C. Chamon et al., Study of the effects of Pauli blocking and Pauli nonlocality on the optical potential. Nucl. Phys. A **753**, 83–93 (2005). doi: 10.1016/j.nuclphysa.2005.01.031

[45] A.T. Rudchik, A.A. Rudchik, O.O. Chepurnov et al., ^{6}Li + ^{15}N interaction at $E_{c.m.}$ = 23.1 MeV: Validation of the α + d cluster model of ^{6}Li. Phys. Rev. C **103**, 044614 (2021). doi: 10.1103/PhysRevC.103.044614

[46] A.A. Rudchik, A.T. Rudchik, G.M. Kozeratska et al., ^{7}Li + ^{11}B elastic and inelastic scattering in a coupled-reaction-channels approach. Phys. Rev. C **74**, 034608 (2005). doi: 10.1103/PhysRevC.72.034608